Experimental investigation of planar delamination behaviour of composite laminates under Out-Of-Plane loading

Tu, W.; Pascoe, J.A.; Alderliesten, R.C.

Publication date
2023

Document Version
Final published version

Published in
Proceedings of the 31st symposium of ICAF - the International Committee on Aeronautical Fatigue and Structural Integrity

EXPERIMENTAL INVESTIGATION OF PLANAR DELAMINATION BEHAVIOUR OF COMPOSITE LAMINATES UNDER OUT-OF-PLANE LOADING

W.J. Tu[1*], J.A. Pascoe[1] and R.C. Alderliesten[1]

[*]w.tu@tudelft.nl
[1] Department of Aerospace Structures & Materials, Faculty of Aerospace engineering
Delft University of Technology, Kluyverweg 1, 2629HS, Delft, The Netherlands

Abstract: Delamination growth is a key damage mode threatening the structural integrity of fibre reinforced polymer composite structures. To guide design and damage management of composite structures, research efforts have been made to understand delamination behaviours and establish standardized evaluation methods based mainly on one-dimensional delamination tests. However, as most delamination growth in real structures will be planar, the question arises whether these approaches are adequate to evaluate planar delamination behaviour.
In this study, a novel experimental method was developed to investigate the planar delamination behaviour under quasi-static out-of-plane loading. The planar central loaded split (PCLS) specimen was designed to investigate the planar delamination behaviour under mode II loading condition. By analysing digital image correlation (DIC) and C-scan data, the delamination progress was monitored. An acoustic emission (AE) system was used to capture the initiation of damage and to identify different damage types.
The planar delamination growth was found to be dependent on the stacking sequence and interface properties. Additionally, it was found that positioning a rubber mat between the indenter and the specimen prevented the occurrence of delaminations at undesired interfaces. The artificially embedded delamination propagated in the direction to which the fibre orientation of the layer above the crack interface was parallel, but migrated initially to an upper interface at the place where the fibre was perpendicular. A constant increase in the load was observed even though the delamination propagated. The significant drop of loading seen at the end of the test was attributed to the substantial surface cracking.
The research results provide a clearer understanding of the mechanisms of planar delamination under out-of-plane loading. Furthermore, combining with the experimental results, numerical simulation will be conducted to characterize planar delamination behaviour qualitatively and quantitatively, thus to establish a more reliable assessment method for planar delamination growth

Keywords: Planar delamination, Stiffness degradation, Delamination migration, Mode II fracture

INTRODUCTION

As has been discussed in several studies, delamination initiation and evolution in carbon fibre reinforced polymer (CFRP) composite laminates is one of the most typical damage modes that is critical to the reduction of residual strength, thus threatening the integrity of aerospace structures [1]–[3]. In order to provide valuable references for engineering design, it is essential to comprehend the mechanisms of delamination growth in CFRP laminates. Based on both experimental and analytical approaches, test standards have been established to identify the interlaminar fracture toughness of delamination growth under different loading modes [4]–[6]. However, since these methods are simplified to create delamination growth of unidirectional laminates in only one direction, the determined fracture toughness may not be adequate to describe delamination behaviours in real structures, where delamination growth is planar.

Several external factors can be influential to the fracture toughness of delamination growth. The geometry of the beam specimen, its width [7]–[10] and thickness [11], [12], for instance, have effects on the degree of fibre bridging and thus affect the fracture resistance, causing the R-curve behaviour. Although the measurement of delamination growth was simplified in one direction, the strain energy release rate (SERR) distribution along the delamination front can be influenced by the free edges, resulting in an uneven SERR distribution and thus causing a varying crack growth rate at the delamination front [13]–[15]. The stacking sequence of composite laminates is also influential on the delamination behaviours [16]–[19]. Delamination migration has been found to be the most characteristic phenomenon for delamination growth at the $0°/\theta$ ($0°<\theta<90°$) interface, because the local mode III was dominant at the migration location [15], [20].

Instead of considering those effects separately by using beam specimens, research efforts have been made to investigate planar delamination growth of multidirectional CFRP laminates, where all the factors such as specimen configuration, stacking sequence, and interfacial properties should be considered [21]–[24]. Buckle-driven delamination of CFRP laminates with an artificially embedded delamination has received increasing attention during the past few decades [25]–[30]. Experimental, numerical, and analytical methods have been established, in order to determine the critical strain levels for local buckling and delamination growth, respectively [30], [31]. Delamination was found to propagate transverse to the loading direction due to the local buckling deformation. Although these methods provided convenience in predicting the critical load for initial delamination growth, they were not sufficient to predict progressive delamination evolution.

An innovative experimental method has been developed by Cameselle et al. [32] to investigate mode I dominant planar delamination behaviour. In that research, transparent woven GFRP laminates with an embedded delamination were used. The planar delamination patterns of different woven fabric distributions were investigated. By using the cohesive zone modeling (CZM) method, the fracture toughness of the planar delamination growth was estimated, and was found to be 30% higher than that of one dimensional delamination growth in the DCB specimen [33]. In another study, a novel experimental method was proposed to investigate the planar delamination behaviours of CFRP laminates under mode II and mixed mode I/II loading conditions [34]. The embedded delamination developed under fatigue loading for mixed mode I/II tests. A strain energy density (SED) method was proposed based on digital image correlation (DIC) analysis to monitor delamination growth. Combining with a physical SERR approach presented by Amaral et al. [35], [36], two phases of planar delamination growth under fatigue loading were characterized. However, the SED method was only capable of measuring the projected delamination area. The delamination patterns at different interfaces were not depicted.

In this study, a new experimental method is proposed to investigate the planar delamination behaviour of CFRP laminates under quasi-static loading condition. DIC analysis was performed during the loading process to acquire the surface strain and displacement. After loading, ultrasonic scanning (C-scan) was used to capture the delamination area and analyse the delamination patterns of two different specimen configurations. Furthermore, cross-sectional observation was used to verify the delamination patterns

observed by C-scan. An acoustic emission (AE) system was used to determine the initiation of delamination growth, enabling the estimation of the critical loading for delamination growth.

EXPERIMENTAL APPROACH

Material and specimen

A unidirectional carbon fibre / epoxy prepreg, Delta-Preg M30SC-150-DT120-34F, was used to manufacture the CFRP panels. The DT120 epoxy system has been widely used in structural components that require high toughness and high impact resistance performance.

As shown in Figure 1, a planar central loaded split (PCLS) specimen was designed to investigate planar delamination behaviour under mode II loading condition. The PCLS specimens were fully clamped by the fixtures in the hatched area. The out-of-plane loading was applied by an indenter with a slightly curved head. Additionally, a rubber mat was placed in between the indenter and the specimen to provide a more even load on the specimen surface. The specimens with rubber protection are labelled PCLS-R.

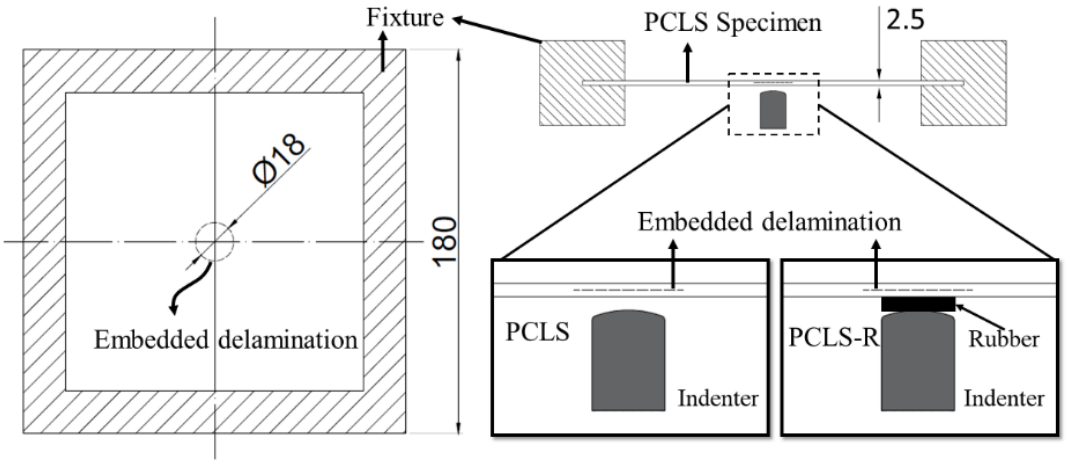

Figure 1: Illustration of the specimen geometry and basic setup.

In order to investigate the effect of interface properties on the delamination behaviour, two different quasi-isotropic layups with 16 layers were adopted. A circular Polytetrafluoroethylene (PTFE) insert of 0.016 mm thickness was embedded in the half thickness. The specimen configurations are described in Table 1. The upper and lower sub-laminates are symmetrical.

Table 1: The specimen configurations (// indicates the location of the PTFE insert).

Label	*Stacking sequence*
PCLS(0//90)	[(0/90/45/-45)s//(90/0/45/-45)s]
PCLS-R(0//90)	[(0/90/45/-45)s//(90/0/45/-45)s]
PCLS-R(0//0)	[(0/90/45/-45)s//(0/90/45/-45)s]

Experimental setup

In order to monitor planar delamination growth, different devices were used. The experimental setup is shown in Figure 2. The specimen was assembled in a fixture that was specifically designed for DIC measurement. The DIC cameras were placed on the top of the crosshead of a 15 kN MTS fatigue testing machine. Four acoustic emission sensors with broad frequency response (Vallen Systeme, VS900-M) were attached to the bottom of the specimen, and connected to a signal acquisition system to detect damage initiation during the loading process.

Once the test started, the DIC and AE systems were triggered to continuously acquire images and AE signals throughout the whole test. The loading rate was set at 0.01mm per second, with DIC images

taken every 5 seconds. After testing, the extended delamination area was depicted through two types of C-scan devices. Ultrasonic scanning equipment developed in the TU Delft laboratory was used to capture the projected delamination area, based on through transmission attenuation. While the C-scan device provided by DolphiTech, Inc. enabled time of flight (TOF) illustration of the delamination area through the depth of the specimen (as shown in the blue region in Figure 2). The specimens were scanned from the bottom side, where out-of-plane loading was applied. Finally, the specimens were cut into pieces for cross-sectional observation.

The tests were performed under displacement control. The tests were interrupted after significant surface cracking occurred, in order to prevent the specimens from being penetrated by the indenter. The significant surface cracking was therefore considered as failure of the specimens.

Figure 2: Illustration of the specimen geometry and basic setup.

RESULTS

Force-displacement curves

The force-displacement curves are shown in Figure 3 Compared to PCLS without rubber protection, PCLS-R specimens exhibit softened force-displacement behaviour. The force-displacement behaviours of PCLS-R specimens with different stacking sequences are similar. The drops in the force-displacement curves indicate the occurrence of significant surface cracking (failure). The failure of PCLS(0//90) occurred at a lower displacement level compared to PCLS-R(0//90). However, the stiffness degradation due to delamination growth is not visible in the force-displacement curves, the force increased exponentially until failure.

According to the compliance analysis, a continuous stiffening process can be discovered for all specimens, as shown in Figure 4. The compliance of the specimen decreased even though the embedded delamination propagated. The peaks in the compliance curves indicate the occurrence of surface cracking, as shown in Figure 4(b). For PCLS (0//90), one significant surface crack occurred close to the end of loading. For PCLS-R(0//90), multiple surface cracks developed at a lower displacement level. Only barely visible surface cracking happened in PCLS-R(0//0). The occurrence of surface cracking has a significant impact on the compliance curves. In contrast, a stiffness degradation (compliance increase) due to growth of the delaminations is not visible.

Planar delamination behaviour

The inspected delamination patterns for all specimens are shown in Figure 5. The delamination areas captured by the two different C-scan devices matched. The C-scan results on the left were acquired by differentiation of penetrated signal strength, providing the projected delamination shapes. Through TOF C-scan, delaminations at different interfaces (depths) were illustrated in different colours. It is worth mentioning that since the specimen thickness is 2.5 mm, the darker orange colour corresponds to the mid interface (1.25 mm depth) where the initial delamination was embedded. The top surface where DIC measurement was performed was set as the back wall, as shown in dark blue colour.

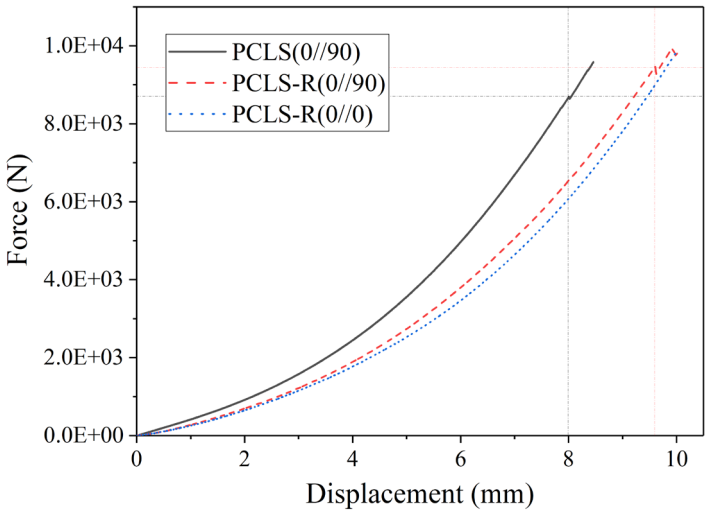

Figure 3: Force-displacement curves of all specimen configurations. The thin dash-dot lines are used to mark the critical force and displacement of failure.

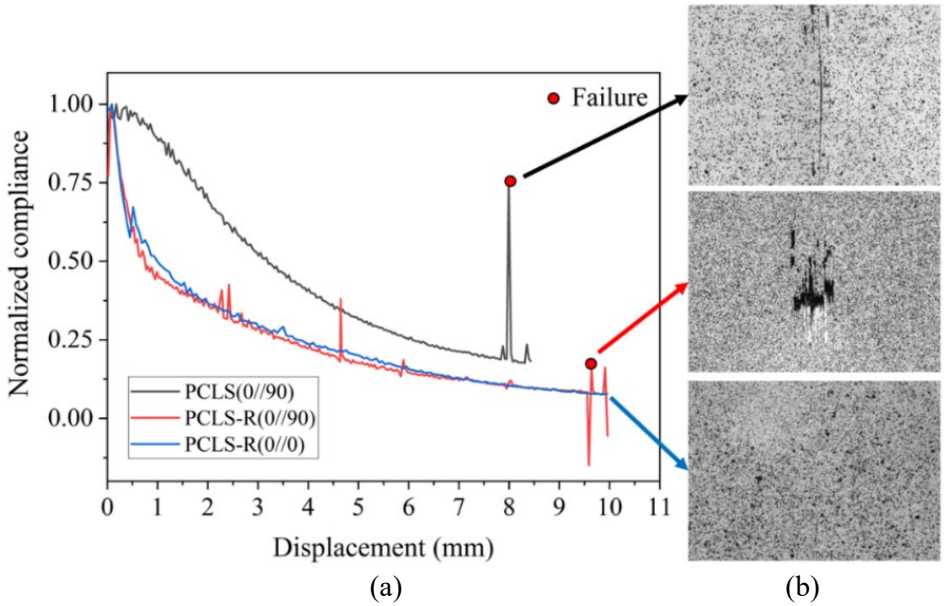

Figure 4: (a)Compliance curves of all specimen configurations and (b)Surface cracking

For PCLS(0//90) without rubber protection, multiple delaminations occurred at undesired interfaces. For the specimens with rubber protection (PCLS-R), two main delamination regions can be recognized. First, a rectangular delamination area, shown in dark orange colour, illustrates the initial delamination growth following the ply orientation above the mid interface. Second, the two semi-sphere regions, shown in light orange colour, depict the delamination at an upper interface. Such delamination behaviour indicates that the initial delamination propagated along the fibre orientation above the mid interface but migrated in the direction where the normal direction of the initial delamination boundary was perpendicular to

the fibre orientation. Comparing the rectangular delamination regions of PCLS-R specimens, the delamination growth at the middle 0//0 interface was smaller than that at the middle 0//90 interface, although the two specimens were loaded to the same displacement and force level.

For PCLS-R(0//0), another smaller delamination region attached to the side of the rectangular region can be observed, as shown in navy blue. This area depicts the delamination underneath the cracked top surface. The same delamination growth at the top interface can be observed from the TOF C-scan of PCLS(0//90). Similar delamination behaviour can also be expected for PCLS-R(0//90). However, the top-interface delamination was totally shadowed by the mid-interface delamination because the TOF C-scan was performed from the back side.

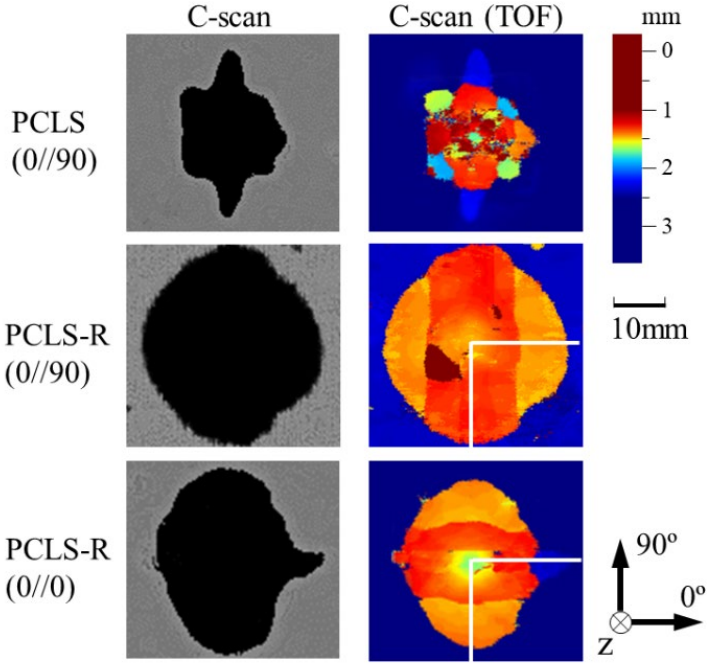

Figure 5: C-scan depicted delamination patterns of all specimen configurations. The white solid lines indicate the cutting lines for the cross-sectional observations. The color bar on the right illustrates the measured depth based on the TOF.

In order to provide more insights into the observed delamination behaviour, cross-sectional observation was conducted on PCLS-R specimens. As shown in Figure 6, the embedded delamination propagated in the direction where the normal direction of the delamination boundary aligned with the fibre orientation above the mid interface (blue lines), but jumped to an upper interface at the location where the normal direction was perpendicular to the fibre orientation (orange lines). The migrated delamination growth again followed the fibre orientation of an upper ply.

The interface properties can be influential to the planar delamination behaviour. For the PCLS-R(0//0) specimen, the interface of initial delamination growth was 0//0, but the interface of migrated delamination growth was 0//90. As can be observed from the TOF C-scan, different degrees of delamination growth occurred at two adjacent interfaces, resulting in an elliptical shape. For PCLS-R(0//90), the interfaces of both initial and migrated delamination growth were the same. This could result in the self-similar delamination growth observed from the TOF C-scan. The original circular delamination developed roughly into a round shape.

However, it was not clear whether the middle plane delamination or the migrated delamination propagated first or how the interface properties could affect the planar delamination behaviour. The mechanisms of the observed phenomenon need to be further interpreted based on either numerical or analytical analysis.

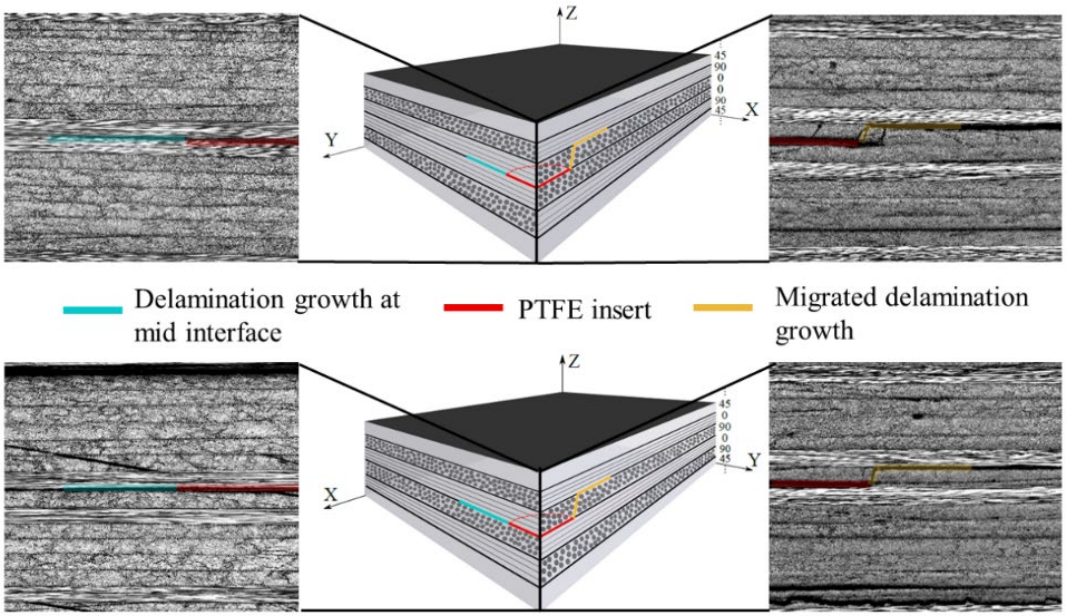

Figure 6: Planar delamination mechanisms observed from two perpendicular cross sections of PCLS-R(0//0) specimen (on the top) and PCLS-R(0//90) specimens (on the bottom).

Monitoring delamination process

The 3D DIC measurement can be a potential approach capable of detecting damage evolution by analysing the surface information [34]. AE technique also provides convenience in monitoring damage initiation [37], [38]. In this study, the two techniques were combined to detect the initiation and propagation of planar delamination under quasi-static indentation.

Two specimen configurations, PCLS-R(0//0) and PCLS-R(0//90) were considered in this analysis. The AE sensor distribution and the locations for extracting the surface properties from DIC analysis are shown in Figure 7. Different sensor distributions, square for PCLS-R(0//0) and parallelogram for PCLS-R(0//90), were considered. The 1, 2 sites for DIC analysis were located aligned with the fibre orientation of the top ply (x axis), while the 3, 4 sites were located along the y axis. Note that the fibre orientation of the top ply was the same as the ply above the mid interface.

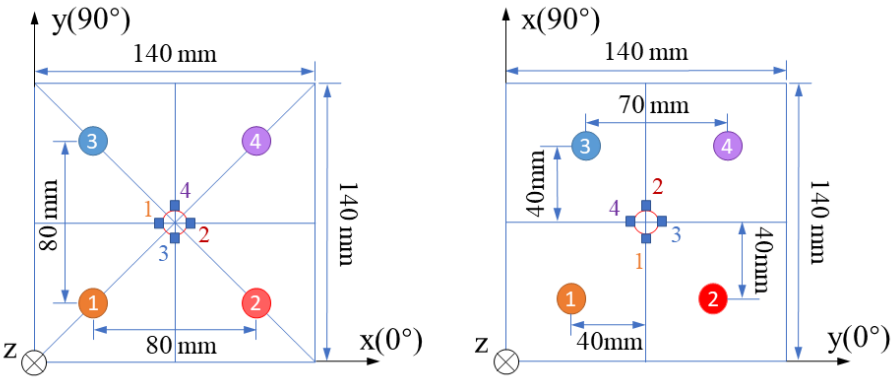

(a) (b)

Figure 7: AE sensor distrubutions (circles) and locations of surface information extraction from DIC analysis (squares) for (a)PCLS-R(0//0) and (b)PCLS-R(0//90) specimens.

As shown in Figure 8 and Figure 9 the surface strain and curvature at the four locations were acquired. For the PCLS-R(0//0) specimen (Figure 8), a nonlinear increase in the surface strain can be observed. Such nonlinear behaviour could be attributed to the minor damage occurring at the surface or inside the specimen. It can be considered the initiation of delamination growth. Especially for mode II dominant

delamination growth, the propagation of delamination is a result of the coalescence of microcracks in the vicinity of the delamination front [39].

According to the surface curvature (Figure 8(b)), a plateau stage occurred after applying 7 mm displacement at locations 3, 4, indicating the propagation of planar delamination. However, the plateau did not exist at locations 1, 2. Instead, larger nonlinear behaviours in the surface curvature can be recognized at locations 1, 2. The sudden drops after 9 mm displacement at these two sites corresponded to significant surface cracking along the fibre orientation at the top ply. The extracted surface curvature evolution can be correlated to the observed planar delamination behaviour. At locations 1, 2 aligned with the top ply orientation, smaller delamination growth but significant surface cracking was observed. At locations 3, 4, transverse to the top ply orientation, a larger delamination area developed.

As shown in Figure 9(a), for PCLS-R(0//90), the nonlinear phase of the surface strain occurred at a lower displacement level at locations 3, 4. This can be attributed to the occurrence of multiple surface cracks. As for the surface curvature (Figure 9(b)), the plateau stage existed at all four locations and only shifted a little in the displacement. This demonstrated that the delamination behaviours in the x and y directions were identical, as evidenced by the C-scan result, which showed a circular delamination area. The curvature fluctuation at the lower displacement level can be caused by the occurrence of multiple surface cracks.

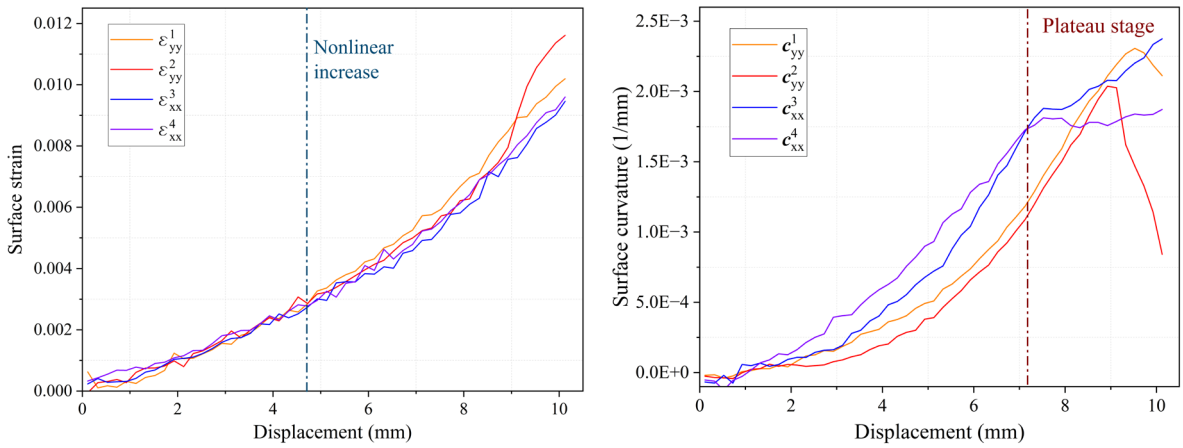

(a) (b)

Figure 8: Surface strain (a) and curvature (b) plots against the applied displacement at four locations for PCLS-R(0//0).

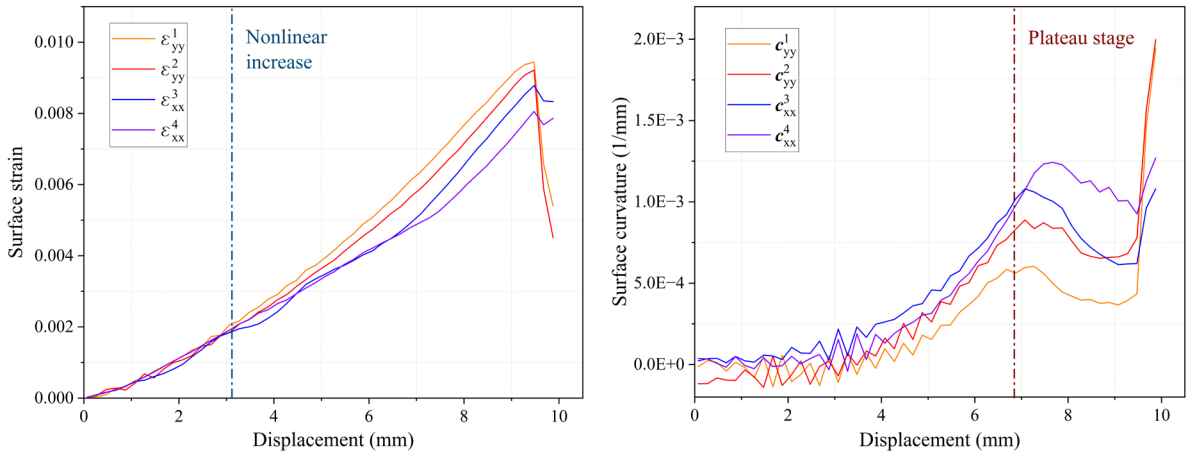

(a) (b)

Figure 9: Surface strain (a) and curvature (b) plots against the applied displacement at four locations for PCLS-R(0//90).

However, the results of DIC analysis can be influenced by surface damage. The nonlinear behaviour in the surface strain curve can be caused by surface damage instead of internal damage. Therefore, it is not sensitive enough to accurately detect the initiation of delamination. The surface curvature is sensitive to the occurrence of delamination growth, but is insufficient to determine the initiation of delamination growth. AE, on the other hand, is in principle capable of detecting any kind of damage occurring in the specimen based on feature analysis of the acquired AE events (hits).

As shown in Figure 10 and Figure 11, the AE hits, accumulated AE energy, and counts of all four sensors are plotted against the applied displacement. The accumulated AE energy and counts are on a magnified scale in order to highlight the sudden increases in the gradient.

As shown in Figure 10, for PCLS-R(0//0), more AE hits were recorded by sensor 2 in the range of 5 mm to 7 mm displacement compared to the other sensors. However, the curves of accumulative AE energy and counts of each sensor were approximately the same. AE hits with high amplitude were recorded by all the sensors at a lower displacement level. These events could be considered the occurrence of the initial debonding between the layers and the PTFE insert at the middle interface. As specified by the black arrows, the displacement levels corresponding to the first significant increase in the gradient of the accumulative AE energy were almost the same for all sensors. However, there was no obvious sudden increase in the accumulated AE counts. Therefore, the first significant increase in the gradient of the accumulative AE energy can be used as an indicator of the initiation of the embedded delamination growth. Similar results can be obtained for the PCLS-R(0//90) specimen (Figure 11).

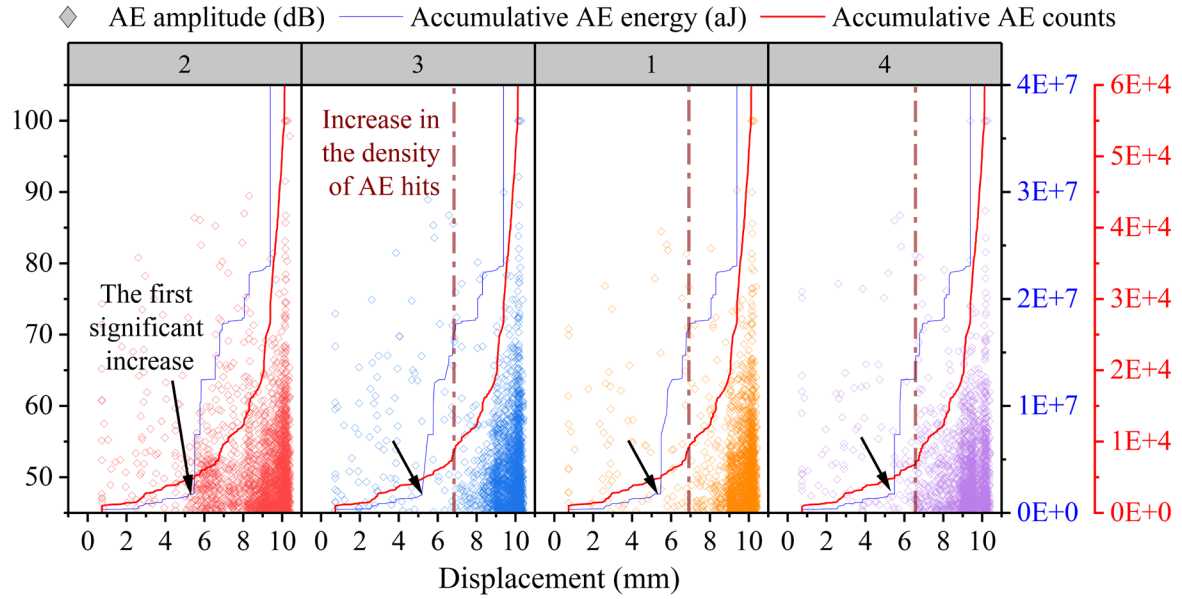

Figure 10: AE hits, accumulated AE energy and counts of each sensor plotted agains the applied displacement for PCLS-R(0//0).

The critical displacements for the initiation of the embedded delamination growth as determined by the AE were 5.5 mm for PCLS-R(0//0) and 4.0 mm for PCLS-R(0//90). The critical displacements were higher than that, which corresponded to the nonlinear phase in the surface strain curves. The displacement corresponding to the sudden increase in the density of AE hits for both specimens was closely matched to the displacement corresponding to the plateau stage in the surface curvature. Therefore, these features can be considered the propagation of delamination growth. The critical displacements for delamination propagation in PCLS-R specimens were around 7 mm.

Further analysis of the clustering of the AE hits and damage localization needs to be performed, in order to identify the damage types and localize the damage based on the AE signals. The results can be verified with fractographic observation at the crack surface. By achieving this, AE can be developed as a

powerful tool capable of performing more accurate damage detection and structural health monitoring (SHM) for real scale structures [40], [41].

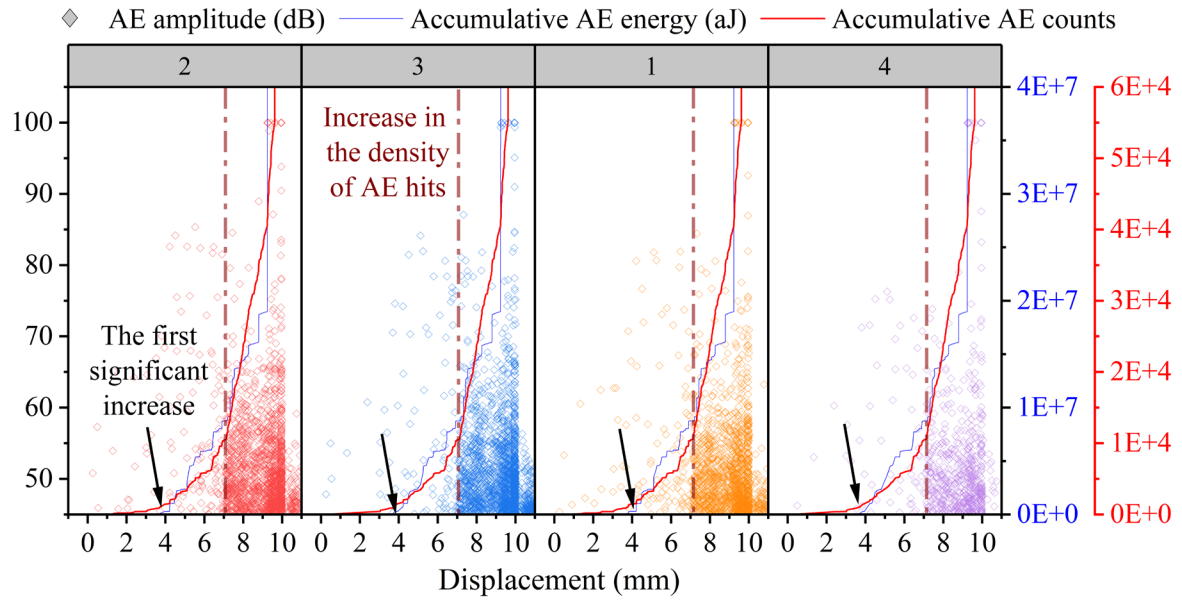

Figure 11: AE hits, accumulated AE energy and counts of each sensor plotted agains the applied displacement for PCLS-R(0//90).

DISCUSSION

Stiffening mechanisms

By analysing the force-displacement behaviour, a continuous stiffening process before the final failure was discovered for all specimens. The stiffness degradation due to delamination growth was not reflected in the force response and was not able to be characterized by the compliance curve. Therefore, it was not possible to calculate the energy dissipation (or energy release rate) based on the force-displacement behaviour or compliance method as suggested in the 1-D test standards.

In 1-D experiments, the stiffening phenomenon is always attributed to the occurrence of fibre bridging [42]–[46]. However, in the presented 2-D experiment, whether there were bridging fibres at the delaminated interface is not clear, because they cannot be easily observed. The degree of bridging effects on planar delamination behaviour is also questionable. In the mode I 2-D delamination experiment, conducted by Cameselle et al. [32], in-plane stretching and fibre bridging were considered the two main stiffening mechanisms. However, since the specimen was not fully constrained on the edges, the stretching effects on the stiffening process were covered by the softening process due to the larger area of delamination growth. In the current study, a larger stretching effect can be expected since the edges of the specimen were fully constrained. This would result in much higher elastic energy storage compared to the energy dissipation due to delamination growth, thus resulting in stiffening behaviour.

In order to reveal the stiffening mechanisms, qualitative and quantitative analysis of the planar delamination behaviour needs to be performed. This would require a numerical or analytical method that is able to calculate the strain/stress state, or energy state at the delamination front.

Planar delamination mechanisms

In mode II delamination, the delamination growth can be considered a consequence of the coalescence of microcracks at the resin rich region between two adjacent plies [39], [47]. The occurrence of microcracks can be influenced by the interface properties and thus affect the delamination behaviour. As shown in Figure 6, for the initial 0//0 interface, in the direction of delamination growth, the micro

matrix cracks between the middle two plies may not be prone to developing since the strong fibres carry a huge amount of loading (stretching effect). For the initial 0//90 interface, the fibre orientation of the bottom ply was parallel to the matrix cracking plane, allowing matrix cracks to extend in the lower ply, which made matrix cracking between the two middle plies easier to develop. The coalescence of multiple matrix cracks resulted in delamination growth aligning with the upper ply orientation since the cracks were not able to propagate across the strong fibres. Therefore, delamination was easier to propagate along the upper ply orientation at 0//90 interface, resulting in a larger delamination area as observed by TOF C-scan in Figure 5.

Additionally, the difference in the amount of resin distributed at different interfaces could affect the occurrence of matrix cracking, thus affecting the delamination behaviour under the mode II dominant loading condition. Since nesting of fibres could occur for the 0//0 interface, less resin could be distributed between the two neighbouring plies, resulting in a thicker overall ply. For 0//90 interface, since the two layers are crossed, more resin could be distributed between the two layers. The micro matrix cracks would occur more easily in the region where more resin is distributed, thus resulting in more delamination growth at 0//90 interfaces. However, in order to confirm the assumptions, detailed microscopic observation needs to be conducted to observe the evolution of matrix cracks at the interfaces.

CONCLUSION

In this study, an experimental method was proposed to investigate mode II dominant planar delamination behaviour under quasi-static out-of-plane indentation. The planar delamination patterns were depicted through ultrasonic scanning techniques. DIC and AE were used to detect the initiation and propagation of an embedded circular delamination. Cross-sectional observation was also performed to explore the mechanisms of planar delamination behaviour. The following conclusions can be drawn:

- Based on the force-displacement and compliance analysis, a continuous stiffening process was observed. The load drops in the force-displacement curves corresponded to the surface cracking. However, the stiffness degradation due to delamination growth is not visible in the force-displacement or compliance curves.
- The embedded circular delamination would propagate aligning with the fibre orientation of an upper ply above the delaminated interface. Migration would occur in the direction where the fibre orientation was perpendicular to the direction of delamination growth. The interface properties have an impact on the planar delamination behaviour, resulting in a difference in the area of delamination growth at different interfaces in composite laminates.
- The surface strain from DIC analysis is not sensitive enough to detect the initiation of the embedded delamination growth. The plateau stage of surface curvature curves can represent the occurrence of delamination propagation. Accumulated AE energy provided reasonable estimations of the critical displacement levels for both the initiation and propagation of the embedded planar delamination.

By combining different measurement methods, the mechanisms of planar delamination can be interpreted. The planar delamination patterns and the underlying mechanisms have been revealed in the current study. Further qualitative and quantitative analysis needs to be performed to characterize planar delamination behaviour, by achieving which it is promising to develop a more appropriate damage evaluation method for real structures.

REFERENCES

[1] M. J. Suriani, H. Z. Rapi, R. A. Ilyas, M. Petrů, and S. M. Sapuan, “Delamination and manufacturing defects in natural fiber-reinforced hybrid composite: A review,” *Polymers (Basel).*, vol. 13, no. 8, pp. 1–24, 2021.

[2] J.-A. Pascoe, "Slow-growth damage tolerance for fatigue after impact in FRP composites: Why current research won't get us there," *Theor. Appl. Fract. Mech.*, vol. 116, no. August, p. 103127, 2021.
[3] N. Sela and O. Ishai, "Interlaminar fracture toughness and toughening of laminated composite materials: a review," *Composites*, vol. 20, no. 5, pp. 423–435, 198.
[4] ASTM D5528-01, "Standard test method for mode I interlaminar fracture toughness of unidirectional fiber-reinforced polymer matrix composites," *ASTM*, 2014.
[5] ASTM D6671M, "Standard Test Method for Mixed Mode I-Mode II Interlaminar Fracture Toughness of Unidirectional Fiber Reinforced Polymer Matrix Composites," *ASTM*, 2014.
[6] ASTM D7905, "Standard test method for determination of the mode II interlaminar fracture toughness of unidirectional fiber-reinforced polymer matrix composites," *ASTM*, 2014.
[7] A. Jyoti, R. F. Gibson, and G. M. Newaz, "Experimental studies of Mode I energy release rate in adhesively bonded width tapered composite DCB specimens," *Compos. Sci. Technol.*, vol. 65, no. 1, pp. 9–18, 2005.
[8] M. K. Budzik, S. Heide-Jørgensen, and R. Aghababaei, "Fracture mechanics analysis of delamination along width-varying interfaces," *Compos. Part B Eng.*, vol. 215, 2021.
[9] M. D. Kempe *et al.*, "Measurement of crack length in width tapered beam experiments," *J. Adhes. Sci. Technol.*, vol. 35, no. 4, pp. 357–374, 2021.
[10] Y. Zhao, R. Alderliesten, Z. Zhou, G. Fang, J. Zhang, and R. Benedictus, "On the physics of applying finite width and geometry correction factors in fatigue crack growth predictions of GLARE," *Int. J. Fatigue*, vol. 117, pp. 189–195, 2018.
[11] L. P. Canal, M. Alfano, and J. Botsis, "A multi-scale based cohesive zone model for the analysis of thickness scaling effect in fiber bridging," *Compos. Sci. Technol.*, vol. 139, pp. 90–98, 2017.
[12] G. Frossard, J. Cugnoni, T. Gmür, and J. Botsis, "Composites : Part A Mode I interlaminar fracture of carbon epoxy laminates : Effects of ply thickness," *Compos. Part A*, vol. 91, pp. 1–8, 2016.
[13] A. Møberg, M. K. Budzik, and H. M. Jensen, "Crack front morphology near the free edges in double and single cantilever beam fracture experiments," *Eng. Fract. Mech.*, vol. 175, pp. 219–234, 2017.
[14] D. Daniewicz and G. Frantziskonis, "Edge delamination in laminated composites," *Compos. Struct.*, vol. 21, no. 3, pp. 141–153, 1992.
[15] N. Pichler, M. Herr, J. Botsis, M. Herráez, and J. Botsis, "Mixed-mode fracture response of anti-symmetric laminates: Experiments and modelling," *Compos. Part B Eng.*, vol. 197, 2020.
[16] Y. Gong, L. Zhao, J. Zhang, and N. Hu, "Crack closure in the fatigue delamination of composite multidirectional DCB laminates with large-scale fiber bridging," *Compos. Struct.*, vol. 244, 2020.
[17] L. Zhao *et al.*, "An interface-dependent model of plateau fracture toughness in multidirectional CFRP laminates under mode I loading," *Compos. Part B*, vol. 131, pp. 196–208, 2017.
[18] J. G. W. N. S. Choi, A. J. Kinloch, "Delamination Fracture of Multidirectional Carbon-Fiber/Epoxy Composites under Mode I, Mode II and Mixed-Mode I/II Loading," 1998.
[19] C. Liu, Y. Gong, Y. Gong, W. Li, Z. Liu, and N. Hu, "Mode II fatigue delamination behaviour of composite multidirectional laminates and the stress ratio effect," *Eng. Fract. Mech.*, vol. 264, p. 108321, 2022.
[20] M. Herráez, N. Pichler, G. A. Pappas, C. Blondeau, and J. Botsis, "Experiments and numerical modelling on angle-ply laminates under remote mode II loading," *Compos. Part A Appl. Sci. Manuf.*, vol. 134, p. 105886, 2020.
[21] G. A. O. Davies and X. Zhang, "Impact Damage Prediction in Carbon Composite Structures," *Int. J. Impact Engng*, vol. 16, no. 1, pp. 149-170, 1995.
[22] G. Davies and P. Irving, "Impact, Post-impact Strength, and Post-impact Fatigue Behavior of Polymer Composites, " *Polymer Composites in the Aerospace Industry*., pp. 303-330, 2019.
[23] M. Sadighi and R. Alderliesten, "Impact fatigue, multiple and repeated low-velocity impacts on FRP composites: A review," *Compos. Struct.*, vol. 297, p. 115962, 2022.
[24] C. Soutis and P. T. Curtis, "Prediction of the post-impact compressive strength of CFRP laminated composites," *Compos. Sci. Technol.*, vol. 56, no. 6, pp. 677–684, 1996.

[25] L. B. Andraju, M. Ramji, and G. Raju, "Snap-buckling and failure studies on CFRP laminate with an embedded circular delamination under flexural loading," *Compos. Part B Eng.*, vol. 214, 2020, p. 108739, 2021.
[26] W. Gong, J. Chen, and E. A. Patterson, "Buckling and delamination growth behaviour of delaminated composite panels subject to four-point bending," *Compos. Struct.*, vol. 138, pp. 122–133, 2016.
[27] A. Riccio, A. Raimondo, F. Di Caprio, and F. Scaramuzzino, "Delaminations buckling and growth phenomena in stiffened composite panels under compression. Part II: A numerical study," *J. Compos. Mater.*, vol. 48, no. 23, pp. 2857–2870, 2014.
[28] M. Naghinejad and H. R. Ovesy, "Calculation of total energy release rate in post-local buckling delamination of composite laminates," *J. Compos. Mater.*, vol. 51, no. 5, pp. 623–635, 2017.
[29] K. F. Nilsson, L. E. Asp, J. E. Alpman, and L. Nystedt, "Delamination buckling and growth for delaminations at different depths in a slender composite panel," *Int. J. Solids Struct.*, vol. 38, no. 17, pp. 3039–3071, 2001.
[30] A. Köllner, M. W. D. Nielsen, J. Srisuriyachot, A. T. Rhead, and R. Butler, "Buckle-driven delamination models for laminate strength prediction and damage tolerant design," *Thin-Walled Struct.*, vol. 161, p. 107468, 2021.
[31] A. Köllner, "Predicting buckling-driven delamination propagation in composite laminates: An analytical modelling approach," *Compos. Struct.*, vol. 266, 2021.
[32] A. Cameselle-Molares, A. P. Vassilopoulos, and T. Keller, "Experimental investigation of two-dimensional delamination in GFRP laminates," *Eng. Fract. Mech.*, vol. 203, pp. 152–171, 2018.
[33] A. Cameselle-Molares, A. P. Vassilopoulos, J. Renart, A. Turon, and T. Keller, "Numerical simulation of two-dimensional in-plane crack propagation in FRP laminates," *Compos. Struct.*, vol. 200, pp. 396–407, 2018.
[34] H. J. den Ouden, "Investigating Planar Delamination Behavior in Carbon Fiber Reinforced Polymer Panels An evaluation of delamination criteria," MSc thesis, Delft University of Technology, http://resolver.tudelft.nl/uuid:e47a4a61-c2ff-45bc-994b-ed6bdd2d47ac, 2020.
[35] L. Amaral, L. Yao, R. Alderliesten, and R. Benedictus, "The relation between the strain energy release in fatigue and quasi-static crack growth," *Eng. Fract. Mech.*, vol. 145, pp. 86–97, 2015.
[36] L. Amaral, R. Alderliesten, and R. Benedictus, "Understanding mixed-mode cyclic fatigue delamination growth in unidirectional composites: An experimental approach," *Eng. Fract. Mech.*, vol. 180, pp. 161–178, 2017.
[37] M. Saeedifar and D. Zarouchas, "Damage characterization of laminated composites using acoustic emission: A review," *Compos. Part B Eng.*, vol. 195, p. 108039, 2020.
[38] R. Ferreira Motta, R. Alderliesten, M. Yutaka Shiino, M. Odila Hilário Cioffi, and H. Jacobus Cornelis Voorwald, "Scrutinizing interlaminar fatigue loading cycle in composites using acoustic emission technique: Stress ratio influence on damage formation," *Compos. Part A Appl. Sci. Manuf.*, vol. 138, 2020.
[39] L. Amaral, R. Alderliesten, and R. Benedictus, "Towards a physics-based relationship for crack growth under different loading modes," *Eng. Fract. Mech.*, vol. 195, pp. 222–241, 2018.
[40] A. Broer, G. Galanopoulos, R. Benedictus, T. Loutas, and D. Zarouchas, "Fusion-based damage diagnostics for stiffened composite panels," *Struct. Heal. Monit.*, vol. 21, no. 2, pp. 613–639, 2022.
[41] B. A. de Castro, F. G. Baptista, and F. Ciampa, "Comparative analysis of signal processing techniques for impedance-based SHM applications in noisy environments," *Mech. Syst. Signal Process.*, vol. 126, pp. 326–340, 2019.
[42] B. F. Sørensen and T. K. Jacobsen, "Large-scale bridging in composites: R-curves and bridging laws," *Compos. Part A Appl. Sci. Manuf.*, vol. 29, no. 11, pp. 1443–1451, 1998.
[43] L. Yao, Y. Sun, R. C. Alderliesten, R. Benedictus, and M. Zhao, "Fibre bridging effect on the Paris relation for mode I fatigue delamination growth in composites with consideration of interface configuration," *Compos. Struct.*, vol. 159, pp. 471–478, 2017.
[44] R. Khan, R. Alderliesten, L. Yao, and R. Benedictus, "Crack closure and fibre bridging during delamination growth in carbon fibre/epoxy laminates under mode i fatigue loading," *Compos. Part A Appl. Sci. Manuf.*, vol. 67, pp. 201–211, 2014.

[45] S. M. Jensen, B. L. V. Bak, J. J. Bender, L. Carreras, and E. Lindgaard, "Transient delamination growth in GFRP laminates with fibre bridging under variable amplitude loading in G-control," *Compos. Part B Eng.*, vol. 225, 2021.
[46] J. Ye *et al.*, "Efficiently determining the R-curve and bridging traction-separation relation of mode I delamination in a simple way," *Compos. Struct.*, vol. 288, p. 115388, 2022.
[47] L. Huo, C. Kassapoglou, and R. C. Alderliesten, "A criterion for predicting delamination growth in composite laminates," *Mater. Des.*, vol. 223, p. 111160, 2022.